THE JOURNAL OF PHYSICAL CHEMISTRY B
A JOURNAL OF THE AMERICAN CHEMICAL SOCIETY

pubs.acs.org/JPCB

Article

# Associated Water Stabilization Mechanism Reconciles the Enigmatic Differential Response of Proteins to a Single Osmolyte

Kuldeep Singh Negi, Tanmoy Khan, and Pratik Sen*

Cite This: https://doi.org/10.1021/acs.jpcb.5c06943

Read Online

ACCESS | Metrics & More | Article Recommendations | Supporting Information

**ABSTRACT:** The complexity of the protein−osmolyte interaction stems from the protein-specific stabilizing effects, challenges that traditional theories fail to address. In the same context, this study uses the associated water stabilization mechanism (AWSM) to investigate sorbitol's effect on papain and bromelain. Through a combination of melting, solvation, and conformational dynamics studies, we investigated the effect of sorbitol on the thermal stability, hydration shell, and internal structure of both proteins. Our findings show that sorbitol retards the dynamics of the protein's associated water, which is caused by the strengthening of water−water and water−protein hydrogen bonds. This, in turn, leads to a retardation in the protein's internal conformational dynamics, suggesting a stronger, more rigid interior and ultimately resulting in thermal stabilization. While both proteins individually follow the AWSM framework, the superior thermal stability of papain over bromelain cannot be explained simply by comparing their absolute dynamics in sorbitol. Instead, a more insightful approach is to consider the relative change in dynamics compared to that of the buffer. Our results demonstrate that papain exhibits a greater extent of retardation in its associated water dynamics, which directly correlates with a higher degree of retardation in its internal conformational dynamics. The greater strengthening of the internal structure leads to its superior thermal stabilization. These findings validate the AWSM framework as a more nuanced approach to understanding protein−osmolyte interactions. Our results highlight the importance of the hydration shell in modulating protein stability and provide a deeper, more mechanistic view of these complex relationships.

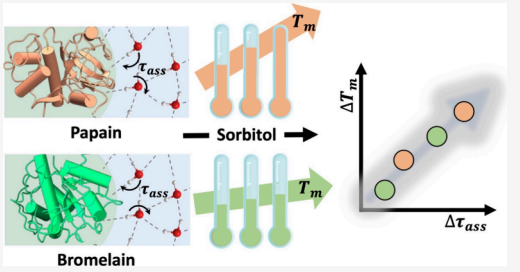




## 1. INTRODUCTION

Proteins are crucial working machinery in living systems. The three-dimensional (3D) structure of the protein plays an important role in defining the functionality of the protein. Under modified environmental conditions, the structure may undergo significant changes that could alter the function of the protein and, in many cases, reduces its effectiveness.[1,2] These changes in the environmental conditions are very common, which includes variations in pH, ionic strength, temperature, and sometimes through incorporation of some solute.[1−3] Nature is smart to sense the possibility of encountering such events and clever to cope with. Under the perturbed environmental conditions, the cell starts accumulating small organic molecules (known as osmolytes) that help the cells to regulate their volume by maintaining the osmotic pressure for optimum activity.[2,4] Osmolytes are broadly of four types: sugars, polyols, amino acids, and methyl amines (and their derivatives). These solutes, along with the task of regulating the cell volume, also stabilize (protect) the protein against the perturbing stresses.[3−11] This aspect of preservation of biomacromolecules by osmolytes has been harnessed in biotechnology and pharmaceutical industries during storage and transport.[12−14] Therefore, a comprehensive understanding of protein−osmolyte interactions is vital, given their biological relevance and industrial utility.

Although several theories have been proposed to explain the protein−osmolyte interactions,[13,15−18] the underlying mechanism is still not fully understood and needs to be revisited in more detail because of its importance. Timasheff and co-workers proposed the initial theory for understanding protein−solute interactions.[16,19−22] They suggested that a protein becomes stabilized when the concentration of the solute on its surface is lower than that in the bulk solution, and the opposite is true when the concentration at the surface is higher. This phenomenon is purely based on the surface tension. Liu and Bolen supported this observation by giving a logical explanation through experimental findings, where they have shown that if the added solute is having repulsive interaction with the protein, the concentration of solute over the surface of the protein will be less than the bulk and in such cases the protein is observed to be stabilized.[23] This theory is known as preferential interaction or a direct interaction mechanism. This theory was insightful but could not explain observation like the thermal stabilization of protein with an increase in glycerol concentration. As per the theory, the surface tension should increase with glycerol

Received: October 8, 2025
Revised: November 24, 2025
Accepted: December 2, 2025

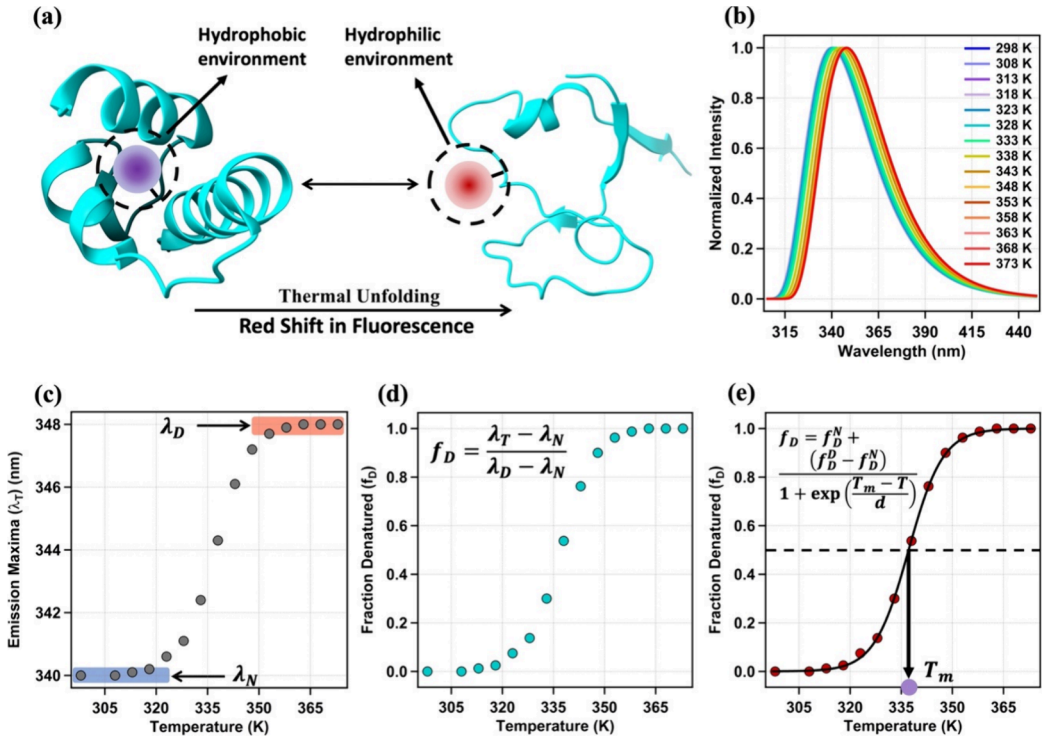


**Figure 1.** (a) Schematic representation of the modulation of emission wavelength representative of a specific distribution of population between native and denatured conformations during protein unfolding in the thermal stability study. Modulation in the (b) normalized emission spectra and (c) emission maxima corresponding to the emission spectra of protein (excited at 295 nm) in buffer with temperature where $\lambda_N$ = 338 nm and $\lambda_D$ = 348 nm are the signature wavelengths for the native and the denatured state of protein in buffer, respectively. (d) Normalized plot representing the fraction of denatured protein at corresponding temperature that has been further (e) fitted with a sigmoidal function represented by eq 2 (provided in the Experimental Procedures) to determine the melting temperature ($T_m$) of the protein.

concentration, but the reverse has been observed experimentally.[24] The other thought for the explanation stems from the hypothesis that water, being present in a large amount, cannot remain passive. It has been noted that proteins tend to be more stable in those osmolyte solutions where the water structure becomes robust by strengthening the hydrogen bonds between water molecules.[25,26] Hishida et al. observed an insightful correlation where the stability of the protein goes parallel with the enhanced water structure.[27] This concept is known as the water structure modulation hypothesis or the indirect mechanism for osmolyte-induced protein stabilization.[26,28−32] While this hypothesis could explain the impact of osmolytes on the thermal stability of proteins in most of the cases, it falls short in accounting for the protein specific effects.

To explain such effects, we hypothesized that the modulation of water associated with the protein is most important and presented the associated water stabilization mechanism (AWSM) for osmolyte induced stabilization of protein.[33−35] It emphasizes the role of water as in the water structure modulation theory, while incorporating the effect of protein as well. Our proposed mechanism explained the thermal stabilization of protein in osmolyte solution very well.[35] The osmolyte that retards the associated water dynamics of the protein stabilizes the protein and vice versa.[35] It helps in understanding the protein specific effect, where the two proteins respond oppositely to an osmolyte. Moreover, to understand the physical origin, the interior flexibility of the protein has been measured using fluorescence correlation spectroscopy (FCS).[36] It has been observed that the thermal stabilization of protein is caused by the strengthening of the interior of the protein, which originates from the osmolyte induced strengthening of the water structure near the protein surface.

In this article, we examined AWSM for protein-specific thermal stabilization in the presence of an osmolyte. An important observation regarding protein-specific effects is the varying degree of stabilization that different proteins experience at a specific concentration of a given osmolyte.[37] This observation has been quantitatively summarized in Table S1 of the SI for clarity. The findings clearly demonstrate that while the modulation of water structure in the bulk caused by the osmolyte may influence the osmolyte−protein interaction, it is not the only contributing factor. We have employed bromelain and papain as the model proteins and sorbitol as the model osmolyte for this study. Our results suggest that both proteins support the hypothesis individually, where thermal stabilization is achieved through the strengthening of the protein's interior, aided by osmolyte-induced stabilization of the water structure near the protein surface. We found that the correlation of absolute values of associated water dynamics and interior flexibility of the protein with its thermal stability may not be sufficient for understanding the different extents of stabilization of proteins in the same osmolyte. Instead, analyzing the changes in these properties in the presence of osmolyte relative to their buffer counterpart is more informative. These findings could advance research in protein science and open new avenues for studying biomacromolecules.

## 2. EXPERIMENTAL PROCEDURES

**2.1. Materials.** We have purchased papain (from papaya latex), bromelain (from pineapple stem), 7-diethylamino-3-(4-


https://doi.org/10.1021/acs.jpcb.5c06943
J. Phys. Chem. B XXXX, XXX, XXX−XXX

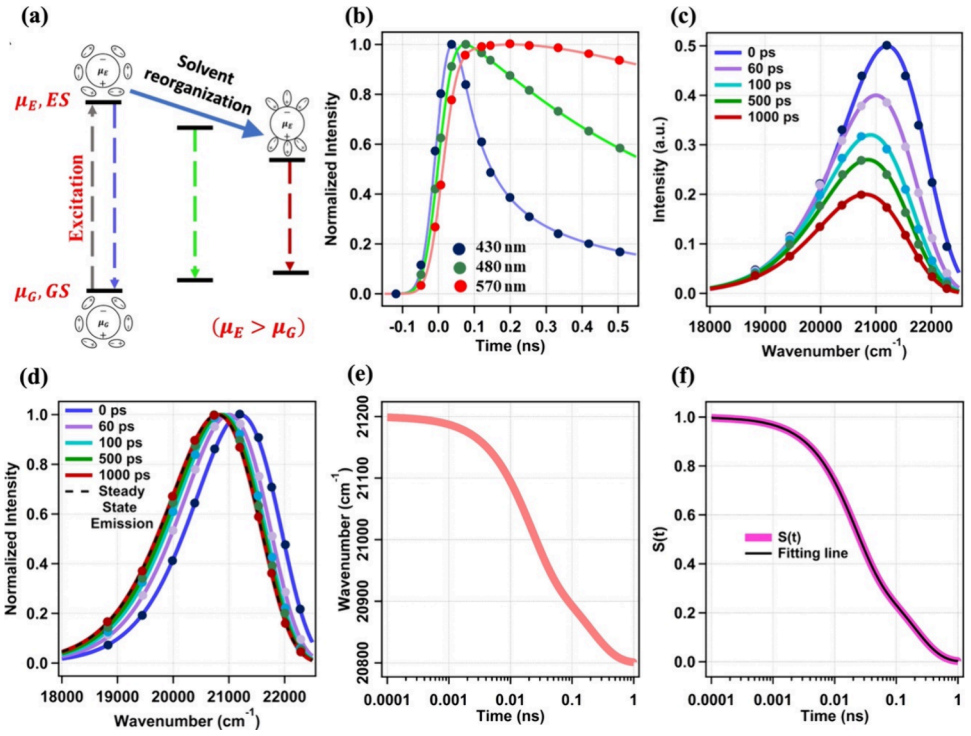


**Figure 2.** (a) Schematic representation of the phenomenon of solvation. (b) Picosecond resolved fluorescent transients of the fluorophore attached protein in buffer. Filled circles and lines represent experimental data and the best multiexponential fit, respectively. Transients display a typical pattern of solvation: fast decay at shorter wavelength and initial rise at longer wavelengths. The fitted parameters are processed along with steady state emission using eq 3 (provided in the Experimental Procedures) to construct the (c) time-resolved emission spectra, and the emission spectrum at each time point is normalized to get the (d) normalized time-resolved emission spectra (TRES) of protein in buffer. The relaxation of the excited state is represented by the (e) variation of the corresponding wavenumber maximum of the representative emission spectra with time and is normalized using eq 4 (provided in the Experimental Procedures) to get the (f) solvent correlation function $S(t)$, which has been further fitted using the biexponential function to obtain the time scales of relaxation of involved processes.

maleimidophenyl)-4-methylcoumarin (CPM) (≥90%), tetramethylrhodamine-5-maleimide (TMR) (≥85%), and D-sorbitol (≥98%) from Sigma-Aldrich and used as received. HPLC-grade dimethyl sulfoxide (DMSO) was purchased from SD Fine Chemicals Ltd. and used after distillation. The dialysis membrane (14 kDa cutoff) was purchased from Sigma-Aldrich and used after washing according to the procedure given by the company. Analytical grade disodium hydrogen phosphate (≥99%) and sodium dihydrogen phosphate (≥98%) were procured from Merck, India, and used directly to prepare 50 mM buffer (pH 7.4). Centrifugal filtration units (10 kDa cutoff, AmiconUltra) were purchased from Merck Millipore, Germany.

**2.2. Protein Labeling.** Papain (PDB ID: 9PAP) and bromelain (PDB ID: 1W0Q) were site-selectively tagged at their only free cysteine residue at the 25th position by a thiol-specific 7-diethylamino-3-(4-maleimidophenyl)-4-methylcoumarin (CPM), as previously described.[35,38,39] The CPM-tagged papain and bromelain are used for steady-state and time-resolved fluorescence measurement. Herein, the solvatochromic nature of CPM was exploited.[35,40] For fluorescence correlation spectroscopic (FCS) measurement, papain and bromelain were tagged with thiol-specific tetramethylrhodamine-5-maleimide (TMR) following established procedures.[35,36]

**2.3. Sample Preparation.** Samples were prepared by mixing the required amount of tagged/untagged papain/bromelain with the required amount of freshly prepared osmolyte stock solution in 50 mM phosphate buffer (pH 7.4). Samples were incubated for 12 h before performing the experiments. Protein concentration was maintained at 10 $\mu$M for steady-state and time-resolved fluorescence. For FCS measurements, the protein concentration was kept at 5 nM.

**2.4. Steady-State Absorption and Emission Measurements.** The steady-state absorption spectra were recorded on a commercial UV−visible spectrophotometer (UV-2450, Shimadzu, Japan) with a built-in temperature controller. The steady-state emission spectra were recorded in a commercial spectrofluorimeter (FluoroMax-4, Jobin Yvon, USA) with a built-in temperature controller.

**2.5. Thermal Study.** Proteins are delicate molecules that can easily change their three-dimensional shape or conformation. This makes them highly sensitive to their surroundings. Any kind of disturbance (like temperature, pressure, pH, salinity, etc.) in their surroundings can modulate the characteristics of the protein.[1−3] This disturbance generally changes the conformation of the protein, and thus, the equilibrium between the folded (native) and unfolded (denatured) population shifts to the right (Figure 1a). In the present work, we have studied the thermal unfolding of a protein employing fluorescence spectroscopy, utilizing the solvatochromic nature of inherently fluorescent amino acid residues (tryptophan). The interior of the protein is hydrophobic, but the surroundings are hydrophilic due to the presence of highly polar water media. During unfolding, the buried tryptophan residues get exposed to water molecules. Owing to the positive solvatochromic nature of the tryptophan, the intrinsic protein fluorescence shifts toward the higher wavelength (red shift), as shown in Figure 1b.[35,41,42] On increasing the temperature, the protein unfolds, and the emission spectra ($\lambda_{ex}$ = 295 nm) shift toward the higher


https://doi.org/10.1021/acs.jpcb.5c06943
J. Phys. Chem. B XXXX, XXX, XXX−XXX

wavelength. A typical plot of the observed emission maximum against the corresponding temperature is presented in Figure 1c, which is generally referred as the melting.[15] From this, the fraction of denatured (unfolded) population at the corresponding temperature is determined using

$$f_D = \frac{\lambda_i - \lambda_N}{\lambda_D - \lambda_N} \quad (1)$$

where $\lambda_i$ represents the emission maximum corresponding to a given temperature, $\lambda_N$ represents the emission maximum of the native state, and $\lambda_D$ represents the emission maximum of the denatured state. A representative plot of $f_D$ against the temperature is shown in Figure 1d.

The melting temperature ($T_m$) of the protein is defined as the temperature at which the population of the folded and unfolded proteins becomes equal, i.e., the temperature corresponds to $f_D = 0.5$ (Figure 1e), which was evaluated through fitting the data set with the sigmoidal function[35,43,44] (black solid line in Figure 1e) as given below.

$$f_D = f_D^N + \frac{(f_D^D - f_D^N)}{1 + \exp\left(\frac{T_m - T}{d}\right)} \quad (2)$$

In the above equation, $f_D^N$ represents the value of the lower asymptote, which is taken as 0 and signifies native state (i.e., $f_D = 0$), $f_D^D$ represents the value of the upper asymptote, which is taken as 1 and signifies the denatured state (i.e., $f_D = 1$), $T_m$ represents the melting temperature, and $d$ is defined as the parameter that is inversely proportional to the slope at the midpoint ($T_m$).[45]

**2.6. Time-Resolved Emission Measurement.** Fluorescence transients at magic angle polarization from the excitation polarization were measured by using a commercial time correlated single photon counting setup (DeltaFlex, Horiba) coupled with a 375 nm pulsed diode laser source. The instrument response function (IRF) of our setup is ~75 ps.

**2.7. Solvation Dynamics Study.** Upon photoexcitation, the dipole moment of a positive solvatochromic dye becomes much larger in its excited state compared to the ground state. As this process is instantaneous, the arrangement of the surrounding solvent molecules in the excited state around the newly created dipole remains the same as that in the ground state, which makes it a thermodynamically unfavorable state. To regain stability, the surrounding solvent molecules reorient their dipoles around the excited-state dipole, and this process is referred as solvent relaxation or solvation, as illustrated in Figure 2a. This rearrangement is usually captured by using time-resolved fluorescence measurements. Fluorescence transients were collected using the TCSPC setup at different wavelengths across the steady-state emission spectrum as schematically represented in Figure 2b. Fluorescence transients were fitted with a sum of exponentials after deconvoluting the IRF. The obtained decay time constants ($\tau_i$) and the corresponding amplitudes ($b_i$) of fluorescence transients were used along with the steady state emission, $F(\lambda)$, to construct the time-resolved emission spectra (TRES, schematically depicted in Figure 2c) using eq 3 (provided in the Experimental Procedures), where $I'(\lambda, t)$ represents the time-dependent intensities at various wavelengths ($\lambda$).

$$I'(\lambda, t) = \frac{F(\lambda)\Sigma b_i \exp\left(-\frac{t}{\tau_i}\right)}{\Sigma b_i \tau_i} \quad (3)$$

The time-resolved emission spectra were normalized by the respective peak intensity to obtain the normalized TRES spectra as shown in Figure 2d. The time evolution of TRES was quantified by its peak shift (Figure 2e) obtained by fitting with a log-normal function, and the solvent correlation function, $S(t)$, was obtained using eq 4 (provided in the Experimental Procedures) as schematically shown in Figure 2f.

$$S(t) = \frac{\bar{\nu}(t) - \bar{\nu}(\infty)}{\bar{\nu}(0) - \bar{\nu}(\infty)} \quad (4)$$

In the above equation, $\bar{\nu}(t)$, $\bar{\nu}0$, and $\bar{\nu}(\infty)$ are the peak position of the TRES at times $t$, 0, and $\infty$, respectively. $S(t)$ was then fitted with a biexponential function to obtain the solvation time components. The average solvation time $\langle\tau_s\rangle$ was calculated as $\langle\tau_S\rangle = a_1\tau_1 + a_2\tau_2$. Further details of the procedure can be found in our previous reports.[41,46]

**2.8. FCS Measurement.** Fluorescence correlation spectroscopy (FCS) measurements were performed on an instrument built in our laboratory. A schematic of the setup and its detailed description can be found in our previous reports.[36,41,47] Briefly, the FCS setup consists of an inverted microscope (IX-71, Olympus, Japan) with a 60× 1.2 NA water-immersion objective (UplanSApo, Olympus, Japan). The sample was kept on a coverslip (Blue Star, Polar Industrial Corporation, India) on the microscope sample platform. A 532 nm (MGL-III-532−5 mW, DreamLaser, China) laser source was used to create a confocal volume 40 $\mu$m above the upper surface of the coverslip. The emitted photons, collected using the same objective, were passed through a dichroic mirror (ZT532rdc, Chroma Tech. Corp., USA, for 532 nm excitation) and an emission filter (605/70m, Chroma Tech. Corp., USA) and then divided into two parts using a 50:50 beam splitter. These two beams are directed to two detectors (SPCM-AQRH-13-FC, Excelitas Tech. Inc., Canada) through a multimode fiber patch chord (M67L01 25/50 $\mu$m 0.10 NA, ThorLabs, USA). The detected signals were correlated using a correlator card (FLEX990EM-12E, correlator.com, USA) and displayed using the LabVIEW platform on a computer. Assuming a Gaussian observation volume and a single component diffusive system without any additional reaction, the fluorescence intensity correlation function can be written as[48]

$$G(\tau) = \frac{1}{N}\left(1 + \frac{\tau}{\tau_D}\right)^{-1}\left(1 + \frac{\tau}{\omega^2\tau_D}\right)^{-1/2} \quad (5)$$

In the above equations, $\tau_D$ is the time constant for diffusion, $N$ is the average number of particles in the observation volume, and $\omega\left(=\frac{l}{r}\right)$ is the ratio of the longitudinal to transverse radius of the 3D Gaussian volume. In the presence of a reaction component with time constant $\tau_R$, which also contributes to the fluorescence intensity fluctuations, the equation is modified to[48]

$$G(\tau) = \frac{1}{N}\left(1 + \frac{\tau}{\tau_D}\right)^{-1}\left(1 + \frac{\tau}{\omega^2\tau_D}\right)^{-1/2}\left(1 + K\exp\left(-\frac{\tau}{\tau_R}\right)\right) \quad (6)$$



https://doi.org/10.1021/acs.jpcb.5c06943
J. Phys. Chem. B XXXX, XXX, XXX−XXX

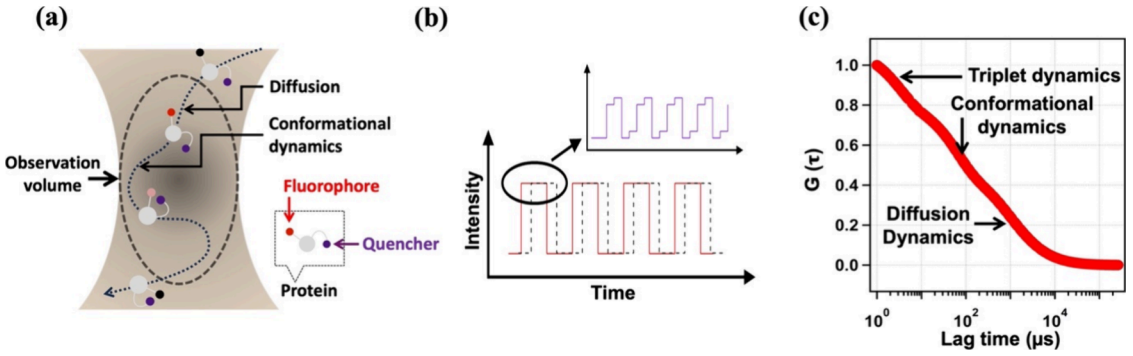


**Figure 3.** Schematic representation of the (a) possible processes of fluorophore attached protein within the observation volume of the FCS setup and the processing of the (b) fluctuations in the emission intensity of the fluorophore attached protein observed by two detectors (one in solid red and other in dotted black, violet color signal represents the fluctuations in the intensity in shorter time scale) to generate the (c) cross-correlation function, $G(\tau)$.

where $K\left( = \frac{k_{AB}}{k_{BA}} = \frac{C_B}{C_A} \right)$ is the equilibrium constant for the reaction $A \rightleftharpoons B$ with forward and backward rate constants of $k_{AB}$ and $k_{BA}$, respectively.[48] If the system exhibits intersystem crossing, one more reaction component ($\tau_T$) will add up and the equation gets modified to

$$G(\tau) = \frac{1}{N}\left(1 + \frac{\tau}{\tau_D}\right)^{-1}\left(1 + \frac{\tau}{\omega^2\tau_D}\right)^{-1/2}\left(1 + K\exp\left(-\frac{\tau}{\tau_R}\right)\right)\left(1 + \frac{p}{1-p}\exp\left(-\frac{\tau}{\tau_T}\right)\right) \quad (7)$$

where $p$ is the fraction of the dye molecules in the triplet state.

We measured several fluorescence intensity correlation curves of rhodamine 6G ($R6G$) at varying concentrations in water and fitted them globally employing eq 5 to determine the value of $\omega$. While calibrating the value of $\omega$, the diffusion coefficient ($D_t$) of $R6G$ in water has been taken to be $4.14 \times 10^{-6}$ cm$^2$ s$^{-1}$.[49] For a particular set of experiments, while fitting the data with eq 6 or 7, the same value of $\omega$ has been used. The value of transverse radius ($r$) of the observation volume is calculated using

$$r = \sqrt{4\tau_D D_t} \quad (8)$$

where $\tau_D$ is the diffusion time and $D_t$ is the diffusion coefficient of the molecule. The observation volume of our FCS setup is estimated to be ~0.6 fL (using 25 $\mu$m fiber patch chord) and ~0.8 fL (using 50 $\mu$m fiber patch chord) using[48,50]

$$V_{eff} = \pi^{3/2} r^2 l \quad (9)$$

where $l = \omega r$ (see Section S1 of the SI for details). In the presence of additives, the refractive index and the viscosity of the solution may change significantly, which needs to be corrected to get the diffusion coefficient. The change in the refractive index is compensated for by changing the objective collar position to achieve the lowest diffusion time value for each of the samples. In this way, we maintain the lowest detection volume attainable for each sample. We have rectified the effects of viscosity changes through performing control experiments at every experimental point taking $R6G$ as the fluorophore. $R6G$ is a rigid molecule and will not undergo any structural changes when exposed to an aqueous solution of additives. In this way, any changes in its diffusion time through the detection volume will be solely due to the differences in the medium viscosity. Using this information and the reported value of the hydrodynamic radius of $R6G$ (7.7 Å) in pH 7.4 buffer, we have calculated the hydrodynamic radius of protein at every experimental point using the following equation.[41,48,50]

$$r_H = r_H^{R6G} \times \frac{\tau_D}{\tau_D^{R6G}} \quad (10)$$

**2.9. Conformational Dynamics Study.** Different processes that are possible in our case with the fluorophore attached protein are illustrated within the representative observation volume (shown in the dark green dotted line) of the FCS setup as shown in Figure 3a. The diffusion of the protein through the observation volume induces fluctuations in the emission intensity with time shown by solid red and black dotted signals recorded separately by two detectors, as shown in Figure 3b. The violet line in Figure 3b shows the fluctuations in each recorded signal at a shorter time scale representative of the modulations in the emission intensity induced by other possible processes like changes in the conformational states of the protein ($A \leftrightarrow B$), triplet state dynamics of the dye. The correlation plot after processing the recording signals is shown in Figure 3c. The time scales of different processes involved in the system are obtained by fitting the correlation plots with an appropriate model. The fitting models are discussed in Section 2.8. The events with dynamics faster than the diffusion dynamics of the fluorophore in the observation volume and slower than the detection limit of the overall FCS setup can be probed only using FCS.

## 3. RESULTS AND DISCUSSION

**3.1. Thermal Stability of Bromelain and Papain in the Presence of Sorbitol.** For bromelain in buffer, the value of $T_m$ is found to be 336 K, which matches well with the literature value.[35,51] With the increase in the sorbitol concentration, the melting curve of bromelain shifts toward the higher temperature values (~338 and ~340 K in the presence of 1 and 2 M sorbitol, respectively), signifying an enhanced thermal stability as shown in Figure 4a and c. For papain, the $T_m$ in buffer is observed as 354 K, which also matches well with the literature value,[35,52] which increases to ~359 K and ~364 K in the presence of 1 and 2 M sorbitol, respectively (Figure 4b and d). All of the data are tabulated in Table 1. The extents of thermal stabilization by osmolyte ($\Delta T_m(Osmolyte) = T_m(Osmolyte) - T_m(Buffer)$) for bromelain and papain are found to be ~2 K and ~4 K, respectively, in the presence of 1 M sorbitol and ~4 K and ~10 K, respectively, in the presence of 2 M sorbitol, as shown in Figure 4e.


https://doi.org/10.1021/acs.jpcb.5c06943
J. Phys. Chem. B XXXX, XXX, XXX−XXX

**Table 1. Variation of the Melting Temperature ($T_m$) and Extent of Change ($\Delta T_m$) in the Melting Temperature of Bromelain and Papain in Buffer and Sorbitol Solution**

| | bromelain | | papain | |
|---|---|---|---|---|
| [sorbitol] (M) | $T_m$ (K) | $\Delta T_m$ (K) | $T_m$ (K) | $\Delta T_m$ (K) |
| 0 | 336.0 ± 0.5 | | 354.4 ± 0.5 | |
| 1 | 338.2 ± 1.0 | 2.2 ± 0.7 | 358.7 ± 0.5 | 4.3 ± 1.1 |
| 2 | 339.6 ± 0.5 | 3.6 ± 1.1 | 364.5 ± 1.0 | 10.1 ± 0.7 |

**3.2. Bulk Water Dynamics in Controlling Protein Stability.** We have clearly observed different extents of sorbitol induced thermal stabilization of bromelain and papain, which is a general observation for most of the osmolytes/additives with different proteins (see Table S1).[37] For example, 2 M sorbitol thermally stabilizes RNase A and $\alpha$-chymotrypsinogen ($\alpha$-CTgen) by ∼12 and ∼7 K, respectively, and 0.75 M inositol thermally stabilizes $\alpha$-CTgen and cytochrome C (Cyt C) by ∼3 and ∼7 K, respectively.

Water structure modulation is considered to derive the thermal stabilization of protein in the presence of osmolytes.[37,53] Recently, Hishida et al. have shown a correlation between the thermal stabilization of RNase A and water structure modulation in the presence of different osmolytes.[27] They found that with the retardation in the bulk water dynamics, the thermal stabilization of the protein increases. Previously, we reported the bulk solvation dynamics of buffer and osmolyte solutions by employing femtosecond transient absorption (TA) spectroscopy. Average bulk solvation dynamics ($\tau_{bulk}$) in water is reported to be ∼0.8 ps, which increases monotonically to 1.1 and 1.6 ps in the presence of 1 and 2 M sorbitol, respectively, as shown in Figure 5a. The data is taken directly from our previous publication, and the details are given in Table S2.[36] In Figure 5b, the extent of thermal stabilization ($\Delta T_m$) is plotted against the change in the average bulk solvation dynamics ($\Delta\tau_{bulk}$). For the individual protein, with the increase in sorbitol concentration, the increase in the extent of retardation in bulk water dynamics is followed by the increase in the extent of thermal stabilization. It signifies the role of bulk water in modulating the thermal stabilization of individual protein in the presence of osmolytes.

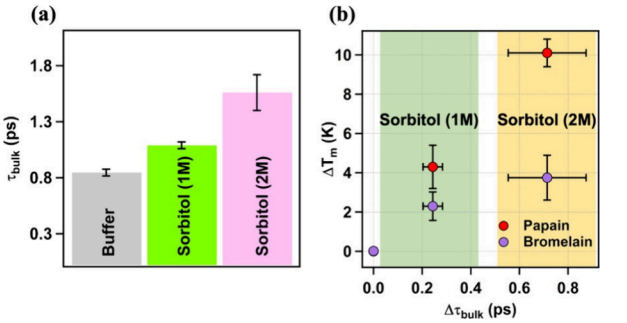


**Figure 5.** (a) Measurement of the bulk solvation dynamics ($\tau_{bulk}$) in buffer, 1, and 2 M sorbitol shown in gray, green, and pink, respectively. Correlation plot showing the variation of (b) the extent of change in melting temperature ($\Delta T_m$) with the extent of change in bulk solvation dynamics ($\Delta\tau_{bulk}$) in the presence of 1 M (green strip) and 2 M (yellow) sorbitol for bromelain (violet) and papain (red).

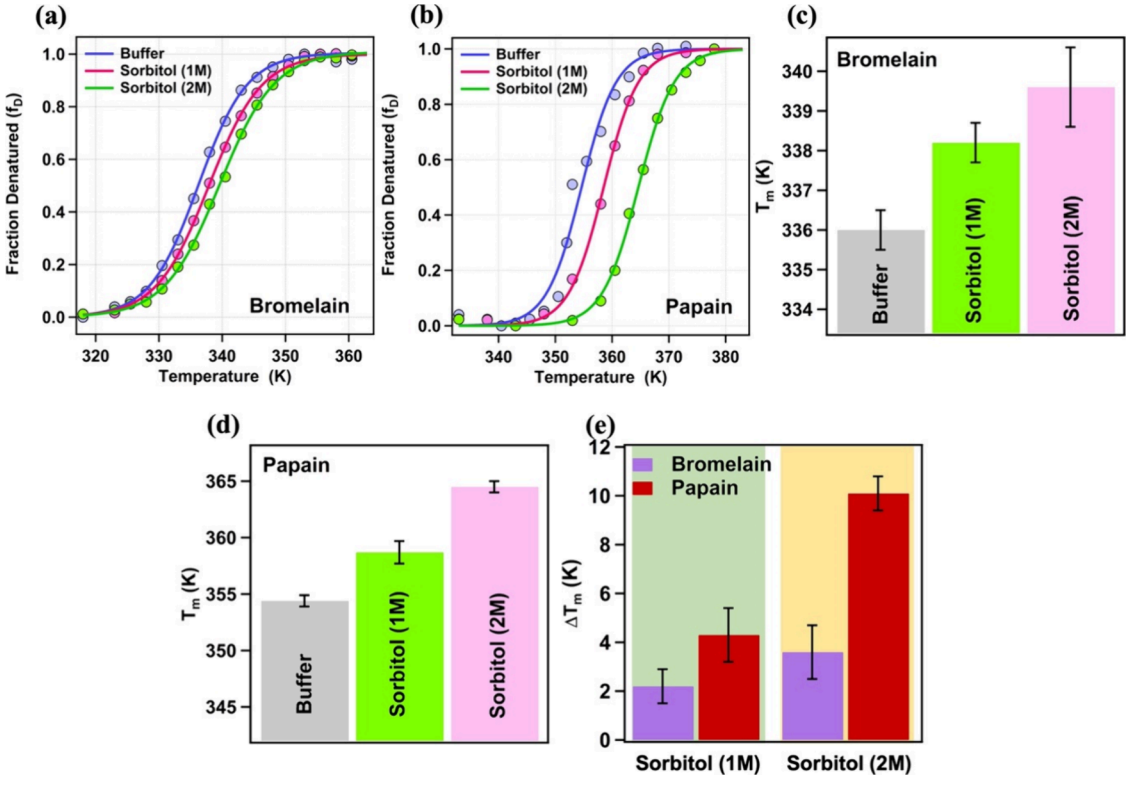


**Figure 4.** Fraction of denatured ($f_D$) (a) bromelain and (b) papain at corresponding temperature in the presence of buffer (violet), 1 M (pink), and 2 M (green) sorbitol along with the fitting line. Variation of the melting temperature ($T_m$) of (c) bromelain and (d) papain in the presence of buffer (gray), 1 M (green), and 2 M (pink) of sorbitol. (e) Increment (relative to buffer counterpart) in the melting temperature ($\Delta T_m$) of bromelain (violet) and papain (red) in 1 M (green) and 2 M (yellow) sorbitol.


https://doi.org/10.1021/acs.jpcb.5c06943
J. Phys. Chem. B XXXX, XXX, XXX−XXX

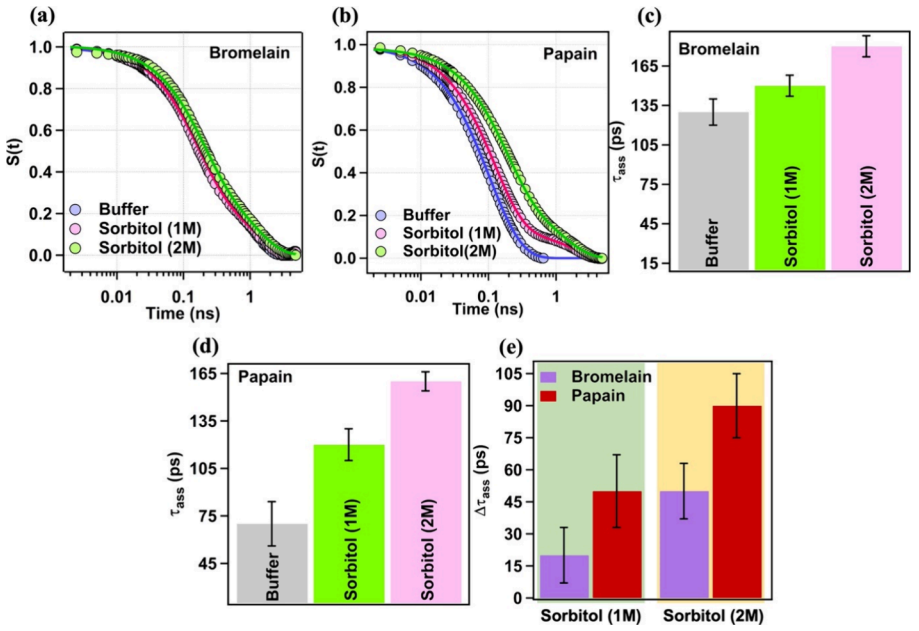


**Figure 6.** Solvent correlation function, $S(t)$ for (a) CPM tag bromelain and (b) CPM tag papain in buffer, 1, and 2 M concentration of sorbitol represented in violet, pink, and green, respectively (dots represent the data and line represent the biexponential fit). Variation of the associated water dynamics ($\tau_{ass}$) of (c) CPM tag bromelain and (d) CPM tag papain in buffer (gray), 1 M (green), and 2 M (pink) sorbitol solution. (e) Increment (relative to buffer counterpart) in the associated water dynamics ($\Delta\tau_{ass}$) of bromelain (violet) and papain (red) in 1 M (green) and 2 M (yellow) sorbitol.

**Table 2. Relaxation Time Constants and Their Relative Weightage in the Solvation Dynamics Study of CPM Tag Bromelain in Buffer and Sorbitol**[a]

| [sorbitol] (M) | $a_1$ | $\tau_1$ (ps) | $a_2$ | $\tau_2$ (ps) | $\tau_{avg}$ (ps) |
|---|---|---|---|---|---|
| 0 | 0.49 ± 0.02 | 130 ± 5 | 0.51 ± 0.02 | 730 ± 19 | 440 ± 3 |
| 1 | 0.64 ± 0.02 | 150 ± 6 | 0.36 ± 0.02 | 990 ± 47 | 450 ± 4 |
| 2 | 0.60 ± 0.02 | 180 ± 7 | 0.40 ± 0.02 | 1100 ± 39 | 550 ± 5 |

[a]Error bar represents the standard deviation of the mean of three independent experiments.

According to the indirect mechanism for osmolyte-induced protein stabilization, as the extent of retardation of water dynamics remains fixed for a given concentration of sorbitol, the extent of thermal stabilization of different proteins is expected to be the same. But it is evident from Figure 5b that for a given $\Delta\tau_{bulk}$ value, the extents of thermal stabilization for papain and bromelain are different. Thus, we can conclude that while bulk water may contribute to osmolyte-induced protein stabilization, it alone cannot account for the thermal stabilization of the two proteins by different extents, and the involvement of additional factors beyond bulk water modulation must be instrumental in the stabilization process.

**3.3. Associated Water Dynamics Modulation in the Presence of Sorbitol.** To further investigate why two different proteins exhibit different levels of thermal stabilization in similar concentrations of the same osmolyte, we examine how the added osmolyte modulates the water that is directly associated with the protein, commonly termed as the associated water or biological water, which reflects influences from both the protein and the osmolyte.[54−59] This water layer is special as it is known to have characteristics that are different from the bulk water and known to vary from protein to protein.[60−64] Apart from the unique behavior of the associated water, it is already evident that this layer also plays a crucial role in defining the properties of the protein.[33,40,59,65−68] Our group reported that the osmolyte modifies the thermal stability of papain by modulating its associated water dynamics.[35] It has been observed that the osmolyte that retards the associated water dynamics thermally stabilizes the protein and vice versa and proposed the associated water stabilization mechanism (AWSM) for the osmolyte induced stabilization of protein.[35] Thermal stabilization of the protein in the presence of different cosolutes is also reported to be influenced by the modulation of the associated water dynamics.[33−35,40,69] It has been shown that Ficoll-70 induced retardation in associated water dynamics stabilizes bromelain via entropy and destabilizes via enthalpy.[40] It has also been illustrated that modulation in the associated water dynamics directly modulates the activity of the protein in the presence of different cosolutes.[33,40]

To test if AWSM can explain the distinct effect of sorbitol on the thermal stabilization of bromelain and papain, we measured the associated water dynamics in both papain and bromelain in the absence and presence of sorbitol. To do this, we covalently attached a solvatochromic fluorophore, 7-diethylamino-3-(4-maleimidophenyl)-4-methylcoumarin (CPM), to the only free cysteine of the proteins. The solvent correlation functions, $S(t)$, for bromelain and papain in the absence and presence of sorbitol along with the fit to a biexponential function are shown in Figure 6a and b, respectively (see Figures S1 and S2 for further details like time-resolved emission spectra, feasibility of the biexponential model over a single exponential model, etc.), and the data are tabulated in Tables 2 and 3.


https://doi.org/10.1021/acs.jpcb.5c06943
J. Phys. Chem. B XXXX, XXX, XXX−XXX

**Table 3. Relaxation Time Constants and Their Relative Weightage in the Solvation Dynamics Study of CPM Tag Papain in Buffer and Sorbitol**[a]

| [sorbitol] (M) | $a_1$ | $\tau_1$(ps) | $a_2$ | $\tau_2$(ps) | $\tau_{avg}$(ps) |
|---|---|---|---|---|---|
| 0 | 0.31 ± 0.15 | 70 ± 14 | 0.69 ± 0.25 | 130 ± 31 | 110 ± 20 |
| 1 | 0.84 ± 0.02 | 120 ± 6 | 0.16 ± 0.02 | 1380 ± 176 | 320 ± 10 |
| 2 | 0.63 ± 0.01 | 160 ± 6 | 0.37 ± 0.01 | 980 ± 43 | 460 ± 20 |

[a]All the data for the solvation dynamics study of CPM tag papain has been procured from our previous work. Error bar represents the standard deviation of the mean of three independent experiments.

Proteins generally show a broad spectrum of solvation events from the picosecond (ps) to nanosecond (ns) range, where the event with a time scale of ∼1 ps originates from the bulk-like water motions.[54,56,70] The ∼5 ps time component comes from the relaxation of the water molecules in the protein hydration layer.[54,60,71] The dynamics in the range of ∼20−200 ps originates from the concerted motions of the protein side chains and the water molecules attached to these side chains on the protein surface.[60,62−64,72] These motions are known to be initiated by the overall network movement of the water molecules in the hydration layer and is known as the associated water dynamics.[62−64] The dynamics >200 ps comes from the various protein motions.[73] As we are interested in probing the associated water layer and specifically the water motion where water and protein both participate, we measured the associated water dynamics ($\tau_{ass}$) in the ∼20−200 ps range using a time dependent fluorescence Stokes shift (TDFSS) technique with a time-correlated single photon counting (TCSPC) system having an instrument response function (IRF) of 75 ps.

For bromelain and papain in buffer, $\tau_{ass}$ values are observed to be 130 (Figure 6c) and 70 ps (Figure 6d), respectively. In the presence of 1 M sorbitol, $\tau_{ass}$ values for bromelain and papain are measured as 150 and 120 ps, respectively. On further increase in the sorbitol concentration to 2 M, the dynamics further retarded to 180 and 160 ps (see Figure 6c and d). To our satisfaction, we observed a strong correlation between $T_m$ and $\tau_{ass}$ for both proteins individually, as depicted in Figure 7a, where the associated water dynamics gets retarded and the protein becomes thermally stabilized. Although both proteins individually adhere to the proposed mechanism (AWSM), the differences in stabilization cannot be directly explained by this theory. To address this, we shift our focus from absolute values to the extent of change ($\Delta\tau_{ass}(Osmolyte) = \tau_{ass}(Osmolyte) - \tau_{ass}(Buffer)$ and $\Delta T_m(Osmolyte) = T_m(Osmolyte) - T_m(Buffer)$), with the goal of better understanding the relative effects of osmolytes on the stabilization of different proteins.

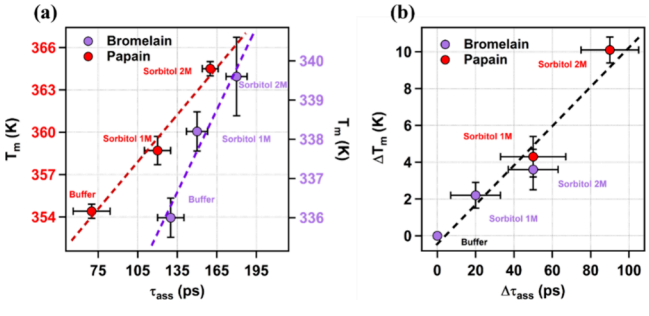


**Figure 7.** Correlation plot showing the variation in the (a) melting temperature ($T_m$) with the associated water dynamics ($\tau_{ass}$) (Adj. $R^2$ for bromelain and papain are 0.88 and 0.96, respectively) and (b) the extent of change in melting temperature ($\Delta T_m$) with the extent of change in associated water dynamics ($\Delta\tau_{ass}$) for bromelain (violet) and papain (red) in the presence and absence of sorbitol (Adj. $R^2$ = 0.92). Filled circles and dotted lines represent the data points and the straight line fit, respectively.

The extents of retardation in the associated water dynamics ($\Delta\tau_{ass}$) for bromelain in the presence of 1 and 2 M sorbitol are estimated to be ∼20 and ∼50 ps, respectively, compared to bromelain in buffer (see Table S3). In the case of papain, these values are estimated to be ∼50 and ∼90 ps, respectively, as shown in Figure 6e (see Table S3). On the other hand, the $\Delta T_m$ values for bromelain in the presence of 1 and 2 M sorbitol are estimated to be 2 and 4 K, respectively. In the case of papain, these values are estimated to be 4 and 10 K, respectively. It is evident that with each of the concentrations of sorbitol, the extent of retardation is less in the case of bromelain than that of papain, i.e., $(\Delta\tau_{ass})_{[X],\ Bromelain} < (\Delta\tau_{ass})_{[X],\ Papain}$ and $(\Delta T_m)_{[X],\ Bromelain} < (\Delta T_m)_{[X],\ Papain}$, where $[X]$ is the concentration of the sorbitol used in this study.

To our delight, the plot of $\Delta T_m$ vs $\Delta\tau_{ass}$ yields a nearly straight line (Figure 7b), indicating that the extent of retardation in the associated water dynamics ($\Delta\tau_{ass}$) is strongly correlated with the extent of the increase in the melting temperature ($\Delta T_m$), which is not a function of the chosen protein.

**3.4. Microsecond Conformational Dynamics Measurement.** In our recent study, we established that osmolyte-induced protein stabilization may originate from a direct relationship between the dynamics of associated water and the internal conformational dynamics of proteins.[36] Stabilizing osmolytes slow both associated water and protein motions, which reduces flexibility and enhances thermal stability. In contrast, destabilizing agents have the opposite effect. This cross-talk between the associated water dynamics and internal protein motions has also been supported by another study.[74] To check if this correlation holds good across the proteins in the presence of the same osmolyte, we have measured the conformational fluctuation time around the active site of bromelain and papain in the absence and presence of 1 and 2 M sorbitol using FCS (see Section 2.9 for details).

In this study, we employed TMR covalently tagged to a free cysteine residue of the protein (CYS 26 in bromelain and CYS 25 in papain) to probe the conformational dynamics. The TMR fluorophore is positioned in close proximity to five tryptophan residues in each protein, leading to a strong fluorescence quenching effect due to the interaction of the $\pi$-electron cloud of the tryptophan side chains. While the quenching is dominated by the nearest tryptophan residue (Trp 27 in bromelain and Trp 26 in papain), all nearby tryptophan residues within the relatively small size of the bromelain ($R_h$ = ∼22 Å) and papain ($R_h$ = ∼18 Å) are expected to influence the signal. This fluorescence quenching is expected to capture the internal dynamics (conformational dynamics) of the protein.[75−77] The TMR dye itself exhibits an inherent triplet state dynamics in the microsecond time scale, which is expected to persist upon covalent attachment to the proteins, albeit with a slight


https://doi.org/10.1021/acs.jpcb.5c06943
J. Phys. Chem. B XXXX, XXX, XXX−XXX

modulation of the absolute value.[48,78] Consequently, the FCS measurements of TMR-tagged bromelain and papain are anticipated to capture a composite of three distinct dynamic events: translational diffusion, protein conformational dynamics reflected by the quenching of TMR fluorescence by the nearby tryptophan amino acid residues, and the intrinsic triplet state dynamics of the TMR dye.

For bromelain in buffer, the cross-correlation function, $G(\tau)$, is best fitted with eq 7 (provided in the Experimental Procedures) and comprises two exponential terms ($\tau_T$ = 5 $\mu$s; $\tau_R$ = 38 $\mu$s) and one diffusion term ($\tau_D$ = 140 $\mu$s). Fitting data are provided in Table 4. Control fitting analyses were performed

**Table 4. Variation of Time Scales of Triplet State Dynamics, Conformational Dynamics, Diffusion Dynamics, and Hydrodynamic Radii of Bromelain in Buffer and Sorbitol Solution**

| [sorbitol] (M) | $\tau_T$ ($\mu$s) | $\tau_R$ ($\mu$s) | $\tau_D$ ($\mu$s) | $R_h$ (Å) |
|---|---|---|---|---|
| 0 | 4.7 ± 0.1 | 38.8 ± 3.9 | 135.9 ± 6.0 | 22.1 ± 1.0 |
| 1 | 4.3 ± 0.3 | 46.3 ± 2.8 | 244.0 ± 10.9 | 20.1 ± 0.9 |
| 2 | 3.5 ± 0.6 | 62.7 ± 3.0 | 548.4 ± 28.8 | 20.2 ± 1.0 |

using alternative models as well, including single-diffusion, dual-diffusion, and single-exponent with diffusion equations to ensure robustness in data interpretation (see Figure S3). Following previous reports, the diffusion term is assigned to the translational motion of TMR-tagged bromelain through the observation volume.[36,75,78] To check the origin of the two exponential terms, we have performed the excitation power dependence and observation volume dependence study. The fast time component found to be independent of excitation power, while the associated amplitude ($p$; see eq 7 provided in the Experimental Procedures) increases steadily with an increase in the excitation power (see Figures S4 and S6). This observation led us to conclude that the origin of this component is the triplet lifetime of the TMR-tag.[48,50,79] The second exponential time component remains unaltered with variation in the excitation power and observation volume (Figures S5 and S7). Following previous literatures,[75,78,80] this time component has been assigned to the conformational dynamics (internal dynamics) of the protein under investigation. In the case of papain in buffer, we also have observed two exponential terms ($\tau_T$ = 6 $\mu$s; $\tau_R$ = 41 $\mu$s) and one diffusion terms ($\tau_D$ = 120 $\mu$s). Following the argument for bromelain and based on our previous control experiments,[36] the observed time constants have been assigned in a similar way as we did for bromelain.

To see how the interior of the two proteins responds in the presence of sorbitol, the FCS study of the bromelain and papain has been performed with 1 and 2 M sorbitol as well. The normalized cross-correlation plots for TMR tag bromelain and TMR tag papain in the presence and absence of sorbitol are shown in Figure 8a and b, respectively. For bromelain and papain in buffer, $\tau_R$ values are observed to be 39 (Figure 8c) and 41 $\mu$s (Figure 8d), respectively. In the presence of 1 M sorbitol, $\tau_R$ for bromelain and papain are measured as 46 and 54 $\mu$s, respectively. On further increase in the sorbitol concentration to 2 M, the dynamics further retarded to 63 and 77 $\mu$s (see Figures 8c and d), respectively. All the data for TMR tag bromelain and papain in the presence and absence of sorbitol are provided in Tables 4 and 5. The continuous increase in the value of $\tau_R$ with increasing sorbitol concentration for both proteins implies retardation in the conformational dynamics or slowness in the inherent motions of the proteins. The observed retardation in protein conformational dynamics can be attributed to two primary factors, modulation in either bulk viscosity or associated water dynamics due to osmolyte addition. However, Frauenfelder et al. demonstrated that large-scale protein motions are governed by solvent viscosity, while small-scale motions are influenced by the properties of water molecules directly

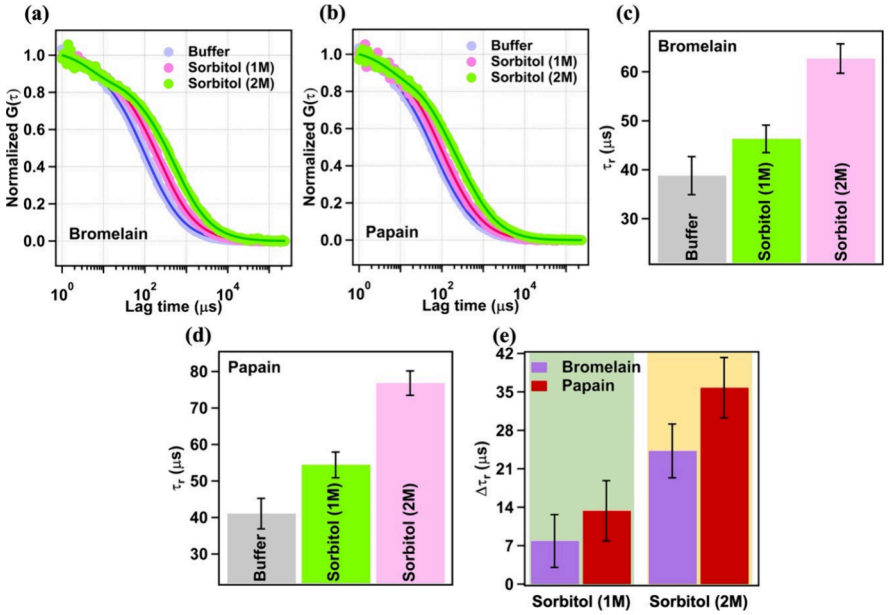


**Figure 8.** Normalized cross-correlation function for (a) TMR tag bromelain and (b) TMR tag papain in buffer, 1, and 2 M sorbitol represented in violet, pink, and green, respectively, along with the fitting line using eq 7 provided in the Experimental Procedures. Variation in the conformational dynamics ($\tau_r$) of (c) TMR tag bromelain and (d) TMR tag papain in buffer, 1, and 2 M sorbitol shown in gray, green, and pink, respectively. (e) Increment (relative to buffer counterpart) in the conformational dynamics ($\Delta\tau_r$) of bromelain (violet) and papain (red) in 1 M (green) and 2 M (yellow) sorbitol.


https://doi.org/10.1021/acs.jpcb.5c06943
J. Phys. Chem. B XXXX, XXX, XXX−XXX

**Table 5. Variation of Time Scales of Triplet State Dynamics, Conformational Dynamics, Diffusion Dynamics, and Hydrodynamic Radii of Papain in Buffer and Sorbitol Solution**

| [sorbitol] (M) | $\tau_T$ ($\mu$s) | $\tau_R$ ($\mu$s) | $\tau_D$ ($\mu$s) | $R_h$ (Å) |
|---|---|---|---|---|
| 0 | 5.9 ± 0.2 | 41.1 ± 4.2 | 119.2 ± 5.0 | 19.4 ± 0.8 |
| 1 | 3.0 ± 0.2 | 54.4 ± 3.5 | 220.1 ± 10.9 | 18.1 ± 0.9 |
| 2 | 4.6 ± 0.1 | 76.8 ± 3.6 | 492.2 ± 31.0 | 18.2 ± 1.2 |

interacting with the protein surface what we refer as associated water.[59,65−67] Our recent findings also demonstrated that while both factors have an impact, the associated water dynamics exert a dominant effect on protein conformational dynamics relative to the bulk viscosity.[36] Based on these, we believe that the observed retardation of the microsecond conformational dynamics in the presence of sorbitol mainly stemmed from the altered associated water in the proteins. The observed retardation in the conformational dynamics could be observed as the result of the strengthened bonding between the amino acids in the interior of the protein.

As expected, we have observed a strong correlation between $\tau_{ass}$ and $\tau_R$ for both of the proteins as depicted in Figure 9a, where the conformational dynamics get retarded with the retardation of the associated water dynamics. The observed correlation provides insight into how sorbitol-induced strengthening of the associated water structure (confirmed by the retardation in associated water dynamics) strengthens the protein's interior (confirmed by the retardation in conformational dynamics), leading to thermal stabilization. Although the two processes are well correlated, even with different time scales of their motions, it is challenging to describe the basis of this correlation. Literature suggests that the motions of proteins at various time scales are interconnected.[81,82] However, without detailed information about protein motions across these time scales, it is difficult to make definitive comments, and this will be the subject of further investigation. Nevertheless, both proteins follow the cross-talk between associated water dynamics and conformational dynamics individually in enhancing thermal stabilization.

However, this correlation does not explain why two different proteins are stabilized to varying degrees with the same concentration of sorbitol. For a better understanding of the relative effects of osmolytes on the stabilization of bromelain and papain, we focused more on the relative change in conformational dynamics ($\Delta\tau_r(Osmolyte) = \tau_r(Osmolyte) - \tau_r(Buffer)$) rather than the absolute values. The extents of retardation in the conformational dynamics ($\Delta\tau_R$) for bromelain in the presence of 1 and 2 M sorbitol are estimated to be 8 and 24 $\mu$s, respectively, compared to bromelain in buffer (see Table S4). In the case of papain, these values are estimated to be 13 and 36 $\mu$s, respectively, as shown in Figure 8e (see Table S4).

It is evident that with each of the concentrations of sorbitol, the extent of retardation is less in the case of bromelain than that of papain, i.e., $(\Delta\tau_r)_{[X],\ Bromelain} < (\Delta\tau_r)_{[X],\ Papain}$, where $[X]$ is the concentration of the sorbitol used in this study. To our delight, the plot of $\Delta\tau_{ass}$ vs $\Delta\tau_r$ yields a nearly straight line (Figure 9b), indicating that the extent of change in the associated water dynamics ($\Delta\tau_{ass}$) is strongly correlated with the extent of change in the conformational dynamics ($\Delta\tau_r$), which is also not a function of the chosen protein. This correlation depicts the less strengthened associated water structure around bromelain compared to papain in the presence of sorbitol, which results in a less strengthened interior of bromelain over papain. To explore how sorbitol induced perturbations in the interior of the two proteins influence their melting thermodynamics, we plotted $\Delta T_m$ against $\Delta\tau_r$ (Figure 9c), depicting that the extent of change in the conformational dynamics ($\Delta\tau_R$) is strongly correlated with the extent of change in the melting temperature ($\Delta T_m$), which is independent of the chosen protein. This correlation shows that the less strengthened interior of bromelain compared to that of papain in the presence of sorbitol results in relatively less thermal stabilization of bromelain over papain.

## 4. CONCLUSIONS

Based on our findings, we propose a better mechanistic understanding of protein-osmolyte interactions, shifting the focus from traditional bulk water theories to the associated water stabilization mechanism (AWSM). Using bromelain and papain as model proteins and sorbitol as the osmolyte, we demonstrated that the associated water dynamics of both proteins get retarded on the addition of sorbitol, which is followed by the retardation in their conformational dynamics. The retardation in associated water dynamics occurs due to the strengthening of water−water and water−protein bonding. This increased stability in the surrounding water shell, in turn, causes a retardation in the protein's conformational dynamics, as it strengthens the interactions between the amino acid residues within the protein

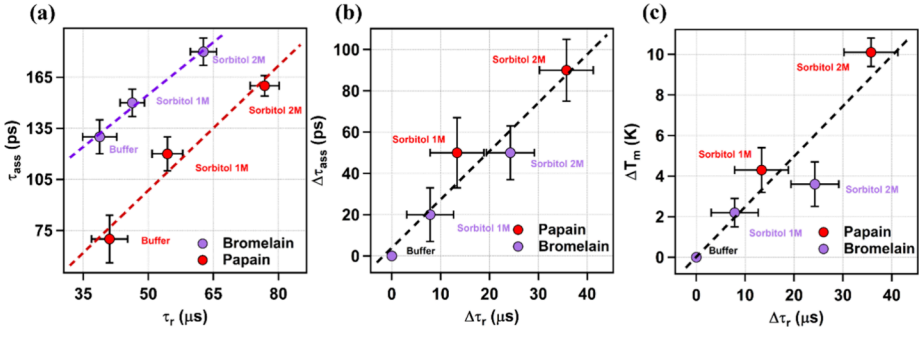


**Figure 9.** Correlation plot showing the variation in the (a) associated water dynamics ($\tau_{ass}$) with conformational dynamics ($\tau_r$) (Adj. $R^2$ for bromelain and papain are 0.98 and 0.91, respectively), (b) extent of change in the associated water dynamics ($\Delta\tau_{ass}$) with the extent of change in the conformational dynamics ($\Delta\tau_r$) (Adj. $R^2$ = 0.90), and (c) extent of change in the melting temperature ($\Delta T_m$) with the extent of change in the conformational dynamics ($\Delta\tau_r$) for bromelain (violet) and papain (red) in the presence and absence of sorbitol (Adj. $R^2$ = 0.80). Filled circles and the dotted lines represent the data points and the straight line fit, respectively.


https://doi.org/10.1021/acs.jpcb.5c06943
J. Phys. Chem. B XXXX, XXX, XXX−XXX

itself. The strengthened interior of each protein in the presence of sorbitol results in its thermal stabilization. However, the degree of thermal stabilization in the presence of sorbitol differs among the two proteins. Papain exhibited a greater extent of retardation in both its associated water and internal dynamics compared to bromelain. This suggests that papain's superior thermal stability is a result of its more significantly strengthened internal structure driven by the sorbitol induced relatively better stabilization of papain's associated water structure over bromelain. This concludes that the disparity could not be explained by simply comparing absolute values but rather by analyzing the extent of change relative to the buffer. Overall, the presented results validate the AWSM framework, offering a deeper, protein-specific view of these interactions that could open new avenues for understanding protein behavior in complex biological environments like in the formation of biomolecular condensates, which are related to neurodegenerative diseases. AWSM is not limited to the studied system and can be employed to understand interactions between different protein−osmolyte systems.

## ■ ASSOCIATED CONTENT

### Supporting Information

The Supporting Information is available free of charge at https://pubs.acs.org/doi/10.1021/acs.jpcb.5c06943.

Plots of solvent correlation function, normalized FCS cross correlation curves, tables of the melting temperature values of proteins, solvation and conformational dynamics (PDF)

## ■ AUTHOR INFORMATION


### Corresponding Author

**Pratik Sen** − *Department of Chemistry, Indian Institute of Technology Kanpur, Kanpur 208016 Uttar Pradesh, India;* orcid.org/0000-0002-8202-1854; Phone: +91 51 2259 6312; Email: psen@iitk.ac.in; Fax: +91 51 2259 6806

### Authors

**Kuldeep Singh Negi** − *Department of Chemistry, Indian Institute of Technology Kanpur, Kanpur 208016 Uttar Pradesh, India;* orcid.org/0000-0002-8395-7937

**Tanmoy Khan** − *Department of Chemistry, Indian Institute of Technology Kanpur, Kanpur 208016 Uttar Pradesh, India;* orcid.org/0000-0003-1101-2827

Complete contact information is available at: https://pubs.acs.org/10.1021/acs.jpcb.5c06943


### Author Contributions

P.S. and K.S.N. conceptualized and visualized the project. K.S.N. performed the experiments and did the analysis. K.S.N. wrote the original draft, and P.S. and T.K. reviewed and edited the manuscript. All the authors actively participated in the discussions. P.S. supervised the work.

### Notes

The authors declare no competing financial interest.

## ■ ACKNOWLEDGMENTS

K.S.N. acknowledges IIT Kanpur for providing the graduate fellowship. T.K. thanks the Prime Minister Research Fellowship (PMRF), Government of India, for the doctoral fellowship. P.S. thanks the Indian Institute of Technology Kanpur for infrastructure and Sanjay & Rachna Pradhan Chair Professor position of IIT Kanpur for support. This work is financially supported by the Science and Engineering Research Board, Government of India (Grant No. CRG/2022/002324).

## ■ REFERENCES


(1) Masson, P.; Lushchekina, S. Conformational Stability and Denaturation Processes of Proteins Investigated by Electrophoresis under Extreme Conditions. *Molecules* **2022**, *27*, 6861.

(2) Steeves, C. L.; Hammer, M.-A.; Walker, G. B.; Rae, D.; Stewart, N. A.; Baltz, J. M. The glycine neurotransmitter transporter GLYT1 is an organic osmolyte transporter regulating cell volume in cleavage-stage embryos. *J. Cell. Physiol.* **2005**, *100* (24), 13982−13987.

(3) Boob, M. M.; Sukenik, S.; Gruebele, M.; Pogorelov, T. V. TMAO: Protecting proteins from feeling the heat. *Biophys. J.* **2023**, *122*, 1414−1422.

(4) Burg, M. B.; Ferraris, J. D. Intracellular organic osmolytes: Function and regulation. *J. Biol. Chem.* **2008**, *283*, 7309−7313.

(5) Yancey, P. H. Organic osmolytes as compatible, metabolic and counteracting cytoprotectants in high osmolarity and other Stresses. *J. Exp. Biol.* **2005**, *208*, 2819−2830.

(6) Canchi, D. R.; Garciá, A. E. Backbone and side-chain contributions in protein denaturation by urea. *Biophys. J.* **2011**, *100*, 1526−1533.

(7) Tadeo, X.; López-Méndez, B.; Castaño, D.; Trigueros, T.; Millet, O. Protein stabilization and the hofmeister effect: The role of hydrophobic solvation. *Biophys. J.* **2009**, *97*, 2595−2603.

(8) Mandal, A. K.; Samaddar, S.; Banerjee, R.; Lahiri, S.; Bhattacharyya, A.; Roy, S. Glutamate counteracts the denaturing effect of urea through its effect on the denatured State. *J. Biol. Chem.* **2003**, *278*, 36077−36084.

(9) Diamant, S.; Eliahu, N.; Rosenthal, D.; Goloubinoff, P. Chemical Chaperones Regulate Molecular Chaperones in Vitro and in Cells under Combined Salt and Heat Stresses. *J. Biol. Chem.* **2001**, *276*, 39586−39591.

(10) Kaushik, J. K.; Bhat, R. Why is trehalose an exceptional protein stabilizer? An analysis of the thermal stability of proteins in the presence of the compatible osmolyte trehalose. *J. Biol. Chem.* **2003**, *278*, 26458−26465.

(11) Faria, T. Q.; Lima, J. C.; Bastos, M.; Maçanita, A. L.; Santos, H. Protein stabilization by osmolytes from hyperthermophiles: Effect of mannosylglycerate on the thermal unfolding of recombinant nuclease a from Staphylococcus aureus studied by picosecond time-resolved fluorescence and calorimetry. *J. Biol. Chem.* **2004**, *279*, 48680−48691.

(12) Wlodarczyk, S. R.; Custódio, D.; Pessoa, A.; Monteiro, G. Influence and effect of osmolytes in biopharmaceutical formulations. *Eur. J. Pharm. Biopharm.* **2018**, *131*, 92−98.

(13) Wang, W.; Ohtake, S. Science and art of protein formulation development. *Int. J. Pharm.* **2019**, *568*, No. 118505.

(14) Baskakov, I.; Bolen, D. W. Forcing thermodynamically unfolded proteins to fold. *J. Biol. Chem.* **1998**, *273*, 4831−4834.

(15) Pepelnjak, M.; Velten, B.; Näpflin, N.; von Rosen, T.; Palmiero, U. C.; Ko, J. H.; Maynard, H. D.; Arosio, P.; Weber-Ban, E.; de Souza, N.; Huber, W.; Picotti, P. In situ analysis of osmolyte mechanisms of proteome thermal stabilization. *Nat. Chem. Biol.* **2024**, *20*, 1053−1065.

(16) Lin, T.; Timasheff, S. N. Why do some organisms use a urea-methylamine mixture as osmolyte? Thermodynamic compensation of urea and trimethylamine N-oxide interactions with protein. *Biochemistry* **1994**, *33*, 12695−12701.

(17) Brom, J. A.; Petrikis, R. G.; Pielak, G. J. How Sugars Protect Dry Protein Structure. *Biochemistry* **2023**, *62*, 1044−1052.

(18) Santoro, M. M.; Liu, Y.; Khan, S. M. A.; Hou, L. X.; Bolen, D. W. Increased Thermal Stability of Proteins in the Presence of Naturally Occurring Osmolytes. *Biochemistry* **1992**, *31*, 5278−5283.

(19) Arakawa, T.; Timasheff, S. N. The stabilization of proteins by osmolytes. *Biophys. J.* **1985**, *47*, 411−414.

(20) Timasheff, S. N. Water as Ligand: preferential binding and exclusion of denaturants in protein unfolding. *Biochemistry* **1992**, *31*, 9857−9864.

(21) Noelken, M. E.; Timasheff, S. N. Preferential solvation of bovine serum albumin in aqueous guanidine hydrochloride. *J. Biol. Chem.* **1967**, *242*, 5080−5085.
(22) Lee, J. C.; Timasheff, S. N. The stabilization of proteins by sucrose. *J. Biol. Chem.* **1981**, *256*, 7193−7201.
(23) Liu, Y.; Bolen, D. W. The Peptide Backbone Plays a Dominant Role in Protein Stabilization by Naturally Occurring Osmolytes. *Biochemistry* **1995**, *34*, 12884−12891.
(24) Kumar, V.; Chari, R.; Sharma, V. K.; Kalonia, D. S. modulation of the thermodynamic stability of proteins by polyols: Significance of polyol hydrophobicity and impact on the chemical potential of water. *Int. J. Pharm.* **2011**, *413*, 19−28.
(25) Rezus, Y. L. A.; Bakker, H. J. Destabilization of the hydrogen-bond structure of water by the osmolyte trimethylamine N-oxide. *J. Phys. Chem. B* **2009**, *113*, 4038−4044.
(26) Wirtz, H.; Schäfer, S.; Hoberg, C.; Havenith, M. Differences in Hydration Structure Around Hydrophobic and Hydrophilic Model Peptides Probed by THz Spectroscopy. *J. Infrared Millim. Terahertz Waves* **2018**, *39*, 816−827.
(27) Hishida, M.; Anjum, R.; Anada, T.; Murakami, D.; Tanaka, M. Effect of Osmolytes on Water Mobility Correlates with Their Stabilizing Effect on Proteins. *J. Phys. Chem. B* **2022**, *126*, 2466−2475.
(28) Funkner, S.; Havenith, M.; Schwaab, G. Urea, a structure breaker? Answers from THz absorption spectroscopy. *J. Phys. Chem. B* **2012**, *116*, 13374−13380.
(29) Senske, M.; Törk, L.; Born, B.; Havenith, M.; Herrmann, C.; Ebbinghaus, S. Protein stabilization by macromolecular crowding through enthalpy rather than entropy. *J. Am. Chem. Soc.* **2014**, *136*, 9036−9041.
(30) Bellissent-Funel, M. C.; Hassanali, A.; Havenith, M.; Henchman, R.; Pohl, P.; Sterpone, F.; Van Der Spoel, D.; Xu, Y.; Garcia, A. E. Water Determines the Structure and Dynamics of Proteins. *Chem. Rev.* **2016**, *116*, 7673−7697.
(31) Hishida, M.; Kaneko, A.; Yamamura, Y.; Saito, K. Contrasting Changes in Strongly and Weakly Bound Hydration Water of a Protein upon Denaturation. *J. Phys. Chem. B* **2023**, *127*, 6296−6305.
(32) Higuchi, Y.; Saleh, M. A.; Anada, T.; Tanaka, M.; Hishida, M. Rotational Dynamics of Water near Osmolytes by Molecular Dynamics Simulations. *J. Phys. Chem. B* **2024**, *128*, 5008−5017.
(33) Khan, T.; Das, N.; Bhowmik, S.; Negi, K. S.; Sen, P. Critical Role of Water beyond the Media to Maintain Protein Stability and Activity in Hydrated Deep Eutectic Solvent. *J. Phys. Chem. B* **2025**, *129*, 162−175.
(34) Das, N.; Tarif, E.; Dutta, A.; Sen, P. Associated Water Dynamics Might Be a Key Factor Affecting Protein Stability in the Crowded Milieu. *J. Phys. Chem. B* **2023**, *127*, 3151−3163.
(35) Negi, K. S.; Das, N.; Khan, T.; Sen, P. Osmolyte induced protein stabilization: modulation of associated water dynamics might be a key factor. *Phys. Chem. Chem. Phys.* **2023**, *25*, 32602−32612.
(36) Negi, K. S.; Rana, S.; Khan, T.; Mondal, D.; Sen, P. Interplay of protein fluctuation and associated water dynamics in osmolyte-induced stabilization. *Biophys. J.* **2025**, *124*, 2082−2091.
(37) Kaushik, J. K.; Bhat, R. Thermal Stability of Proteins in Aqueous Polyol Solutions: Role of the Surface Tension of Water in the Stabilizing Effect of Polyols. *J. Phys. Chem. B* **1998**, *102* (36), 7058−7066.
(38) Mohan, V.; Sen, P. Elucidation of active site dynamics of papain and the effect of encapsulation within cationic and anionic reverse micelles. *Spectrochim Acta A Mol. Biomol Spectrosc* **2018**, *200*, 202−211.
(39) Das, N.; Khan, T.; Subba, N.; Sen, P. Correlating Bromelain's activity with its structure and active-site dynamics and the medium's physical properties in a hydrated deep eutectic solvent. *Phys. Chem. Chem. Phys.* **2021**, *23*, 9337−9346.
(40) Khan, T.; Halder, B.; Das, N.; Sen, P. Role of Associated Water Dynamics on Protein Stability and Activity in Crowded Milieu. *J. Phys. Chem. B* **2024**, *128*, 8672−8686.
(41) Lakowicz, J. R. *Principles of Fluorescence Spectroscopy*; 3rd ed.; Springer: New York, USA, 2006, DOI: .
(42) Loving, G. S.; Sainlos, M.; Imperiali, B. Monitoring protein interactions and dynamics with solvatochromic fluorophores. *Trends Biotechnol.* **2010**, *28*, 73−83.
(43) Robic, S. Mathematics, Thermodynamics, and Modeling to Address Ten Common Misconceptions about Protein Structure, Folding, and Stability. *CBE—Life Sci. Educ.* **2010**, *9*, 189−195.
(44) Li-Blatter, X.; Seelig, J. Thermal and Chemical Unfolding of Lysozyme. Multistate Zimm-Bragg Theory Versus Two-State Model. *J. Phys. Chem. B* **2019**, *123*, 10181−10191.
(45) Harris, R. S.; Hess, D. R.; Venegas, J. G. An Objective Analysis of the Pressure-Volume Curve in the Acute Respiratory Distress Syndrome. *Am. J. Respir. Crit. Care Med.* **2000**, *161*, 432−439.
(46) Horng, M. L.; Gardecki, J. A.; Papazyan, A.; Maroncelli, M. Subpicosecond measurements of polar solvation dynamics: Coumarin 153 Revisited. *J. Phys. Chem.* **1995**, *99*, 17311−17337.
(47) Subba, N.; Tarif, E.; Sen, P.; Biswas, R. Subpicosecond Solvation Response and Partial Viscosity Decoupling of Solute Diffusion in Ionic Acetamide Deep Eutectic Solvents: Fluorescence Up-Conversion and Fluorescence Correlation Spectroscopic Measurements. *J. Phys. Chem. B* **2020**, *124*, 1995−2005.
(48) Krichevsky, O.; Bonnet, G. Fluorescence correlation spectroscopy: the technique and its applications. *Rep. Prog. Phys.* **2002**, *65*, 251−297.
(49) Müller, C. B.; Loman, A.; Pacheco, V.; Koberling, F.; Willbold, D.; Richtering, W.; Enderlein, J. Precise measurement of diffusion by multi-color dual-focus fluorescence correlation spectroscopy. *Epl* **2008**, *83*, 46001.
(50) Bacia, K.; Haustein, E.; Schwille, P. Fluorescence correlation spectroscopy: principles and applications. *Cold Spring Harbor Protoc.* **2014**, *7*, 709−725.
(51) Kumar, P. K.; Jha, I.; Venkatesu, P.; Bahadur, I.; Ebenso, E. E. A Comparative study of the stability of stem bromelain based on the variation of anions of imidazolium-based ionic liquids. *J. Mol. Liq.* **2017**, *246*, 178−186.
(52) Sathish, H. A.; Kumar, P. R.; Prakash, V. Mechanism of solvent induced thermal stabilization of papain. *Int. J. Biol. Macromol.* **2007**, *41*, 383−390.
(53) Canepa, J.; Torgerson, J.; Kim, D. K.; Lindahl, E.; Takahashi, R.; Whitelock, K.; Heying, M.; Wilkinson, S. P. Characterizing osmolyte chemical class hierarchies and functional group requirements for thermal stabilization of proteins. *Biophys. Chem.* **2020**, *264*, No. 106410.
(54) Pal, S. K.; Peon, J.; Zewail, A. H. Biological water at the protein surface: dynamical solvation probed directly with femtosecond resolution. *Proc. Natl. Acad. Sci. U. S. A.* **2002**, *99*, 1763−1768.
(55) Peon, J.; Pal, K.; Zewail, A. H. Hydration at the surface of the protein monellin: Dynamics with femtosecond resolution. *Proc. Natl. Acad. Sci. U. S. A.* **2002**, *99*, 10964−10969.
(56) Bhattacharyya, S. M.; Wang, Z. G.; Zewail, A. H. Dynamics of Water near a Protein Surface. *J. Phys. Chem. B* **2003**, *107*, 13218−13228.
(57) Kamal, J. K. A.; Zhao, L.; Zewail, A. H. Ultrafast hydration dynamics in protein unfolding: human serum albumin. *Proc. Natl. Acad. Sci. U. S. A.* **2004**, *101*, 13411−13416.
(58) Qiu, W.; Zhang, L.; Okobiah, O.; Yang, Y.; Wang, L.; Zhong, D.; Zewail, A. H. Ultrafast solvation dynamics of human serum albumin: Correlations with conformational transitions and site-selected recognition. *J. Phys. Chem. B* **2006**, *110*, 10540−10549.
(59) Frauenfelder, H.; Chen, G.; Berendzen, J.; Fenimore, P. W.; Jansson, H.; McMahon, B. H.; Stroe, I. R.; Swenson, J.; Young, R. D. A unified model of protein dynamics. *Proc. Natl. Acad. Sci. U. S. A.* **2009**, *106*, 5129−5134.
(60) Mondal, S.; Mukherjee, S.; Bagchi, B. On the origin of diverse time scales in the protein hydration layer solvation dynamics: A molecular dynamics simulation study. *J. Chem. Phys.* **2017**, *147*, No. 154901.
(61) Bagchi, B. *Water in Biological and Chemical Processes: From Structure and Dynamics to Function*; Cambridge University Press: Cambridge, 2013. DOI: .


https://doi.org/10.1021/acs.jpcb.5c06943
J. Phys. Chem. B XXXX, XXX, XXX−XXX

(62) Mukherjee, S.; Mondal, S.; Bagchi, B. Distinguishing dynamical features of water inside protein hydration layer: Distribution reveals what is hidden behind the average. *J. Chem. Phys.* **2017**, *147*, No. 024901.
(63) Qin, Y.; Wang, L.; Zhong, D. Dynamics and mechanism of ultrafast water- protein interactions. *Proc. Natl. Acad. Sci. U. S. A.* **2016**, *113*, 8424−8429.
(64) Qin, Y.; Jia, M.; Yang, J.; Wang, D.; Wang, L.; Xu, J.; Zhong, D. Molecular Origin of Ultrafast Water-Protein Coupled Interactions. *J. Phys. Chem. Lett.* **2016**, *7*, 4171−4177.
(65) Frauenfelder, H.; Fenimore, P. W.; McMahon, B. H. Hydration, slaving and protein function. *Biophys. Chem.* **2002**, *98*, 35−48.
(66) McMahon, B. H.; Frauenfelder, H.; Fenimore, P. W. The role of continuous and discrete water structures in protein function. *Eur. Phys. J. Spec. Top* **2014**, *223*, 915−926.
(67) Fenimore, P. W.; Frauenfelder, H.; McMahon, B. H.; Young, R. D. Bulk-solvent and hydration-shell fluctuations, similar to $\alpha$- and $\beta$-fluctuations in glasses, control protein motions and functions. *Proc. Natl. Acad. Sci. U. S. A.* **2004**, *101*, 14408−14413.
(68) Bhattacharyya, K. Nature of biological water: A femtosecond study. *Chem. Commun.* **2008**, 2848−2857.
(69) Khan, T.; Das, N.; Negi, K. S.; Bhowmik, S.; Sen, P. Understanding the intricacy of protein in hydrated deep eutectic solvent: Solvation dynamics, conformational fluctuation dynamics, and stability. *Int. J. Biol. Macromol.* **2023**, *253*, No. 127100.
(70) Nandi, N.; Bagchi, B. Dielectric Relaxation of Biological Water. *J. Phys. Chem. B* **1997**, *101*, 10954−10961.
(71) Zhang, L.; Wang, L.; Kao, Y.-T.; Qiu, W.; Yang, Y.; Okobiah, O.; Zhong, D. Mapping hydration dynamics around a protein surface. *Proc. Natl. Acad. Sci. U. S. A.* **2007**, *104*, 18461−18466.
(72) Houston, P.; Macro, N.; Kang, M.; Chen, L.; Yang, J.; Wang, L.; Wu, Z.; Zhong, D. Ultrafast Dynamics of Water-Protein Coupled Motions around the Surface of Eye Crystallin. *J. Am. Chem. Soc.* **2020**, *142*, 3997−4007.
(73) Khodadadi, S.; Curtis, J. E.; Sokolov, A. P. Nanosecond relaxation dynamics of hydrated proteins: Water versus protein contributions. *J. Phys. Chem. B* **2011**, *115*, 6222−6226.
(74) Jha, A.; Ishii, K.; Udgaonkar, J. B.; Tahara, T.; Krishnamoorthy, G. Exploration of the correlation between solvation dynamics and internal dynamics of a protein. *Biochemistry* **2011**, *50*, 397−408.
(75) Chattopadhyay, K.; Saffarian, S.; Elson, E. L.; Frieden, C. Measurement of microsecond dynamic motion in the intestinal fatty acid binding protein by using fluorescence correlation spectroscopy. *Proc. Natl. Acad. Sci. U. S. A.* **2002**, *99*, 14171−14176.
(76) Sasmal, D. K.; Mondal, T.; Sen Mojumdar, S.; Choudhury, A.; Banerjee, R.; Bhattacharyya, K. An FCS study of unfolding and refolding of cpm-labeled human serum albumin: Role of ionic liquid. *J. Phys. Chem. B* **2011**, *115*, 13075−13083.
(77) Nandy, A.; Chakraborty, S.; Nandi, S.; Bhattacharyya, K.; Mukherjee, S. Structure, Activity, and Dynamics of Human Serum Albumin in a Crowded Pluronic F127 Hydrogel. *J. Phys. Chem. B* **2019**, *123*, 3397−3408.
(78) Basak, S.; Chattopadhyay, K. Studies of protein folding and dynamics using single molecule fluorescence spectroscopy. *Phys. Chem. Chem. Phys.* **2014**, *16*, 11139−11149.
(79) Gupta, A.; Sankaran, J.; Wohland, T. Fluorescence correlation spectroscopy: The Technique and its applications in soft matter. *Phys. Sci. Rev.* **2019**, *4*, 104.
(80) Chattopadhyay, K.; Saffarian, S.; Elson, E. L.; Frieden, C. Measuring unfolding of proteins in the presence of denaturant using fluorescence correlation spectroscopy. *Biophys. J.* **2005**, *88*, 1413−1422.
(81) Haran, G.; Riven, I. How Fast Dynamics Affect Slow Function in Protein Machines. *J. Phys. Chem. B* **2023**, *127*, 4687−4693.
(82) Buchenberg, S.; Schaudinnus, N.; Stock, G. Hierarchical Biomolecular Dynamics: Picosecond Hydrogen Bonding Regulates Microsecond Conformational Transitions. *J. Chem. Theory Comput.* **2015**, *11*, 1330−1336.




https://doi.org/10.1021/acs.jpcb.5c06943
J. Phys. Chem. B XXXX, XXX, XXX−XXX